Tensor-Based Morphometry reveals structural differences between Down syndrome and Alzheimer's disease mouse model brains

Nick M Powell[1,2], Holly E Holmes[2], Da Ma[1,2], Marc Modat[1], Jorge Cardoso[1], Frances K Wiseman[3], Victor LJ Tybulewicz[4], Elizabeth MC Fisher[3], Mark F Lythgoe[2], and Sebastien Ourselin[1]

[1]Centre for Medical Image Computing, University College London, London, England, United Kingdom, [2]Centre for Advanced Biomedical Imaging, University College London, London, United Kingdom, [3]Department of Neurodegenerative Disease, Institute of Neurology, University College London, London, United Kingdom, [4]MRC National Institute for Medical Research, London, United Kingdom

Introduction Down syndrome (DS), the leading genetic cause of intellectual disability, is caused by trisomy of human chromosome 21 (Hsa21). Individuals with DS have a greater predisposition to Alzheimer's disease (AD), thought to be due to increased dosage of the amyloid precursor protein (APP) gene – an established risk factor for AD[1]. Analysis of mouse models of DS is improving our understanding of the significance of trisomy of Hsa21, and its relationship to AD[2].
The Tc1 mouse[3] and the J20 mouse[4] are, respectively, established models of DS and AD. The Tc1 mouse carries an almost complete copy of Hsa21, but is not functionally trisomic for the APP protein. It thus allows the study of the DS phenotype without the effects of APP trisomy. The J20 mouse expresses a mutant form of APP, as found in familial forms of AD[4], and exhibits key features of human AD, including cognitive decline, synaptic loss and accumulation of amyloid plaques. By crossing Tc1 mice with J20 mice, a novel mouse model has been created – generating four genotypes: wildtype (WT); trisomic (Tc1); APP transgenic (J20), and double mutants: trisomic and APP transgenic (Tc1/J20). Exaggerated behavioural changes and increased plaque load has already been observed in the Tc1/J20 mouse.
We here show the results of a comprehensive morphometric analysis of these mouse brains, to ellucidate structural differences between Tc1, J20 and WT, and between the Tc1/J20 and J20 littermates. We used an optimised protocol for phenotyping mouse brains with high-resolution structural microscopic MRI[5], and a fully automated software pipeline for Tensor-Based Morphometry (TBM), a non-invasive, hypothesis-free technique which covers the entire brain – reducing the need for the laborious delineation of regions of interest – and highlights voxel-wise volume differences between groups, easing the burden of exporatory histology, which is both destructive and time consuming.

Methods *Animals, preparation & image acquisition.* 49 adult male mice (15 Tc1, 14 J20, 8 Tc1xJ20, 12 WT) were bred as previously described[3,4], culled at age 15 months, and perfuse-fixed (20mL 0.9% saline, then 50mL 10% buffered formal saline with 8mM Magnevist). We used a custom 3D printed plastic holder to secure 3 brains at a time, in skull, within a 50ml syringe filled with proton signal-free, non-viscous Fomblin. We employed optimised protocols for structural *ex vivo* µMRI mouse brain phenotyping[5], using an Agilent 9.4T VNMRS, 33mm quadrature birdcage coil (RAPID Biomedical); 11hr 4min spoiled GE3D sequence, with parameters: TE 4.54ms; TR 17ms; flip angle 51°; 6 averages; FOV 32x25x25mm (matrix 800x625x625, 40µm isotropic resolution).
Image processing. We used an automated software pipeline[6] to extract skulls from multi-subject images, orient them to standard space, and non-uniformity correct images. We used a multi-atlas label fusion algorithm, STEPS, to skull-strip brains by propagating masks from an external *ex vivo* atlas database[7,8,9]. Tissues were classified (as grey and white matter, or CSF) using an expectation maximisation algorithm and the freely-available *NiftySeg*, and their volumes added to estimate total intracranical volume (TIV). Intensities were standardised prior to group-wise registration, to avoid individual images dominating the intensity average generated after each iteration. Images were group-wise registered (5 iterations symmetric affine; 20 iterations symmetric non-rigid) using the open-source *NiftyReg* package (*http://cmictig.cs.ucl.ac.uk/research/software*).
Tensor-Based Morphometry. The Jacobian determinant, describing the degree of volumetric change, was calculated at every voxel of the deformation fields resulting from the registration, log-transformmed, and smoothed (Gaussian kernel, FWHM 4 voxels). Voxel-wise statistical tests were performed on these images between groups (Tc1 vs. WT; J20 vs. WT; Tc1/J20 vs. J20), using the general linear model and ANCOVA, with TIV used as a covariate. These were FDR-corrected (q=0.05).

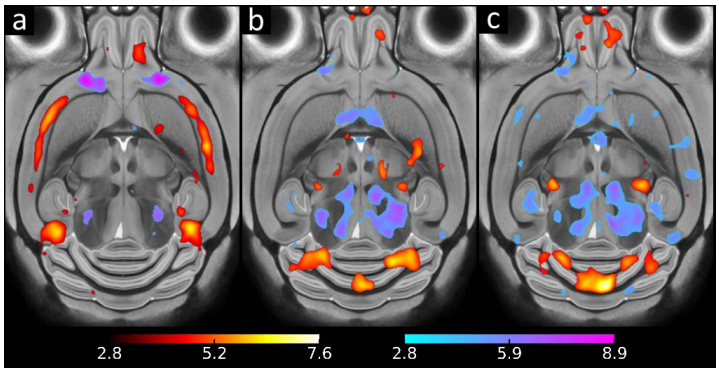

***Figure 1**: statistically significant t-test results (FDR q=0.05) overlaid on the same transverse slice of the final group-wise registration structural average, for three comparisons: (a) J20 vs. WT; (b) Tc1 vs. WT; (c) Tc1/J20 vs. J20. Red: local contraction; blue: local expansion.*

TIV, mm^3	mean	std
TC1	551.993	31.822
J20	495.233	32.094
TC1/J20	542.972	21.481
WT	481.133	11.614

***Table 1**: summary of TIV measurements, in mm^3, for each group, as measured by the sum of the volumes of the segmented tissue classes.*

Results *Brain volume measurements.* Table 1 shows the mean intracranial volumes of each group. Tc1s were significantly grater in volume than WTs ($p<1x10^{-7}$). Tc1/J20s were also significantly greater in volume than than J20s, although to a lesser extent ($p<0.01$). J20s were not significantly larger than WTs ($p=0.16$).
The TBM images reveal local structural differences between these groups' brains.
J20 vs. WT (Fig. 1a). TBM detected bilateral reductions in the J20 group in the cortex, hippocampus, corpus callosum and thalamus.
Tc1 vs. WT (Fig. 1b). The morphometric results indicate extensive central and bilateral reductions in the 5/6 and simple lobules of the cerebellum of the Tc1 group, compared with WTs. Regions of the mid-brain were significantly larger in the Tc1s, but also displayed significant bilateral reductions at foci within the thalamus.
Tc1/J20 vs. J20 (Fig. 1c). Bilateral regions of the cortex, forebrain, hypothalamus and thalamus were significantly larger in the Tc1/J20 group, compared with the J20 animals. We observed a unilateral reduction in the amygdala of the Tc1/J20 group. Lobules of the cerebellum and thalamus remained affected, as in the Tc1 mice. The latter, together with the olfactory bulbs, appeared more extensively affected in the double mutant cohort than the Tc1 group alone compared with WTs.

Discussion We used an optimised µMRI protocol and fully automated software pipeline to investigate the local structural differences between Tc1, J20, Tc1/J20 and WT mouse brains. Within the J20 animals, we observed extensive atrophy in regions vulnerable to amyloid pathology in this model. These findings support the hypothesis linking amyloid plaques and morphometric changes in AD[4]. We have replicated the Tc1 vs. WT results in a younger cohort, lending further credence to this technique. The Tc1/J20 vs. J20 comparison allows us to highlight the regions where the presence of Hsa21 interacts with the J20 AD phenotype, resulting in morphological differences from the APP transgenic mutants alone. Further histological evaluation within these models will explore the biochemical mechanisms underpinning these volume changes, including within the olfactory bulbs, and sub-regions of the thalami of the Tc1/J20 animals. These may also lead to behavioural investigations. Our findings highlight the usefulness of MRI, combined with TBM, for characterising novel phenotypes and informing further studies.

References [1] Oliver, C., & Holland, A. J, (1986) *Psychological Medicine*. 16(2): 307 – 322. [2] Roizen, N. J. & Patterson, D., (2003) *Lancet*. 361(9365): 1281 – 1289. [3] O'Doherty, A., et al., (2005) *Science*. 309 (5743): 2033–2037. [4] Mucke, L. et al., (2000) *Journal of Neuroscience*. 20(11): 4050–4058. [5] Cleary, J.O., et al., (2011) *NeuroImage*. 56(3): 974–983. [6] Powell, N., et al. (2013) *ESMRMB Proceedings* (software) 699. [7] Cardoso, M., et al. (2013). *Medical Image Analysis*, 17(6), 671–84. [8] Ma, D., et al. (2014) *PLOS One*, DOI: 10.1371/journal.pone.0086576. [9] Ma, Y., et al. (2005) *Neuroscience* 135, 1203-1215.